Symmetry and Local Mode Coupling in Absorption and Raman Spectroscopy of Intervalence Electronic Transitions

ARTICLE *in* THE JOURNAL OF PHYSICAL CHEMISTRY A · OCTOBER 2001

Impact Factor: 2.69 · DOI: 10.1021/jp003285a

Symmetry and Local Mode Coupling in Absorption and Raman Spectroscopy of Intervalence Electronic Transitions

David S. Talaga and Jeffrey I. Zink*

Department of Chemistry and Biochemistry,University of California, Los Angeles, Los Angeles, California 90095-1569

Received: September 14, 2000; In Final Form: August 14, 2001

Intervalence electron transfer spectra in mixed-valence molecules are frequently modeled by an interacting pair of adiabatic potential energy surfaces. The presence or absence of a double minimum in the lower surface is correlated with trapped or delocalized charges, respectively. The coordinate involved in this interpretation is the asymmetric normal coordinate representing the nuclear motions taking the molecule from one extreme to the other. In this paper, a model is developed involving both a symmetric and an asymmetric coordinate on an equal footing. The time dependent theory of electronic spectroscopy is used to calculate both absorption and resonance Raman spectra. The model uses physically meaningful interactions in the mixed-valence molecule including the electronic coupling, vibrational coupling, vibrational force constants, and bond length changes as a result of the electron transfer. The effect of these interactions on the relative intensities of symmetric and asymmetric modes in both the absorption and resonance Raman spectra are examined. The quantitative calculations are discussed in parallel with the physical meaning. The calculations show how the spectra can smoothly go from domination by one type of mode to the other. The most important effects are caused by the bond length changes, the electronic coupling, and the force constant changes.

1. Introduction

An intervalence absorption band is caused by a transition that is present in molecules containing two redox centers with different oxidation states. It is absent in molecules where the two sites have the same oxidation state.[1−10] A large number of examples are known where the two sites are metal atoms connected by a bridging ligand.[11−17] A common representation of the transition is shown in Figure 1. This trapped valence picture emphasizes vibrational modes that interchange the molecule from one limiting representation of the location of the charge to the other.[18−22] If the model system depicted above is viewed as nonlinear triatomic molecule, the normal coordinate that is depicted above would be called the asymmetric stretch and the two forms shown at the left and right sides would represent the two limiting extremes of the motion.

This paper is motivated by recent experimental results and theoretical treatments on mixed valence compounds that demonstrate the importance of the symmetric normal coordinate. The necessity of including the symmetric mode is well recognized.[23−26] Recent experimental studies on the Creutz-Taube ion indicate that symmetric bridging vibrations are enhanced in the resonance Raman spectrum of the intervalence band.[27−31] Other observations involving pyrazine-bridged dimers suggest that for valence localized molecules the symmetric pyrazine stretch at 1580−1590 cm^{-1} is present in the IR spectrum but that this band is not present in delocalized systems.[14,15,32] A new class of mixed-valence molecules was proposed (named "class II−III") that have properties associated with both class I (localized) and class III (delocalized in the Robin and Day nomenclature).[1] Resonance Raman studies on other mixed valence iron and ruthenium compounds containing bridging ligands different from pyrazine showed that symmetric modes are enhanced.[16,17] The enhancement of the symmetric mode was interpreted in terms of a three site bonding picture[33−36] because the usual two-state model is based on motions along only an asymmetric coordinate.[18,19] These new studies emphasize the need for a theoretical and interpretive picture that includes both the localized/delocalized extremes and the symmetric and asymmetric normal modes on an equal footing. The model should smoothly carry over from one limiting form to the other.

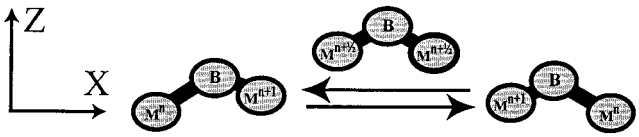

Figure 1. Schematic representation of an intervalence transition between trapped valence states. The coordinate system used in this paper is shown at the left.

The actual motions of large molecules that display intervalence electron-transfer spectra will be distributed over a number of coordinates and will, in general, be much more complicated.[14−17,37,38] Methods for calculating electronic[39−45] and resonance Raman[46,47] spectra involving coupled electronic states and multiple vibrational modes have been developed. However, in considering the symmetry aspects of this problem, the pseudo triatomic picture in Figure 1 is quite useful. This view implicitly assumes that the structure passes through a nuclear configuration having equal bond lengths and that the appropriate point group for discussing the normal coordinates is C_{2v}. This symmetry reveals a disquieting problem: a normal coordinate of motion that is orthogonal to the asymmetric stretch must exist in which both bond lengths are equal and elongate or contract equally and simultaneously (the symmetric stretch.) But this description of the symmetry of the motion is only valid if the equilibrium internuclear bond lengths are equal, a situation that only occurs

10.1021/jp003285a CCC: $20.00
Published on Web 10/27/2001

as the molecule drawn above passes from one limiting form to the other. Of course, the molecule could be interpreted as having equal bond lengths in the ground state (the "delocalized" structure), but then the importance of the asymmetric mode and electron transfer is deemphasized. Contributions from both types of modes are in general possible, and a model that places both modes on an equal footing is required.

This paper explores a model in which both the symmetric and asymmetric modes are treated equally such that there is a smooth transition from one extreme to the other. The model uses two individual "local" metal−ligand modes. The interactions that couple the two local modes to produce the normal coordinates are discussed to provide physical insight. We begin with an overview of the two vibrational coordinate, two electronic state diabatic model which we use to examine simultaneously the factors that influence the relative contributions of the symmetric and asymmetric modes in an intervalence electronic transition. We discuss the various mathematical parameters in the model together with their physical meanings and molecular properties. Following the introduction to the model, we present in brief the procedure used to carry out the calculations using the time-dependent theory of electronic spectroscopy. Then in the next section we examine the influence of the bonding changes and the coordinate dependence of the diabatic coupling on the contribution of the symmetric and asymmetric modes to the *X* polarized absorption and resonance Raman spectra. The trends for *Z* polarization are identical. The final section treats the parameters that are associated with local and normal mode coupling. By exploring these parameters, we determine their influences on the contribution of each mode to the absorption and resonance Raman spectra.

2. The Model for Representing Mixed Valence Species

A. The Diabatic Potential Energy Surface Basis. In general there is no unique way of representing an interacting pair of electronic states.[48,49] However, the coordinate-displaced model provides a simple and natural starting point for representing the intervalence electron transfer.[18,20,21,49] Therefore we will focus our attention on the coupled, trapped valence picture of the diabatics.

The basic ideas of this paper are shown schematically in Figure 2. Before we examine the details of the various forms of coupling and their effects on the potential surfaces and the spectra, we show in broad perspective the basis of the effects that we calculate. In Figure 2, potential surfaces representing the two valence localized forms are labeled A and B. For the moment they are represented as circular wells. One diabatic potential energy surface represents a single valence-localized form of the molecule as shown in Figure 1; the other surface represents the other trapped valence form. The presence of an extra electron results in the two states having equal and opposite distortions in one or more asymmetric coordinates. For simplicity we focus on one of them, the metal-bridging ligand stretch coordinate. The vertical axis represents the M−B coordinate labeled *Q* and the horizontal axis represents the B−M coordinate labeled *R*. Wave packet motion along each of these coordinates represents the appropriate local bond stretching motion.

The intervalence electronic transition places the wave function from one of the surfaces (multiplied by the transition dipole moment) on the other surface. A vertical transition from one state to the other corresponds to moving an electron from one site (M^n) to the other (M^{n+1}) without a change in nuclear position. The vertical transition places the wave packet on the other surface far from its minimum and the wave packet will

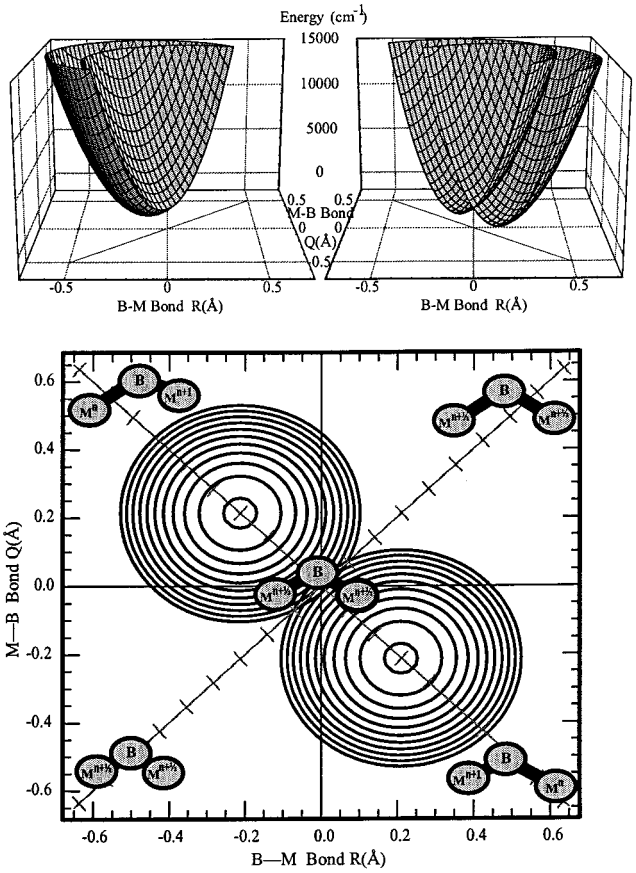

Figure 2. An interacting pair of potentials that forms the basis in which the calculations are carried out (see text). The upper left part illustrates a cross section along the symmetric mode of the two-dimensional diabatics. The upper right part illustrates a cross section along the asymmetric mode. The bottom part is a contour plot of the same potential with illustrations of the bond length distortions arising from different electronic configurations.

evolve in time according to the time-dependent Schrödinger equation. If the motion remains parallel to the line connecting the minima of the two surfaces, the molecular motion is the asymmetric stretch: i.e., one bond elongates while the other contracts. Any motion that develops perpendicular to the line connecting the minima (bisecting the axes) corresponds to the symmetric stretch of the molecule.

Analyzing the forces and interactions in the molecule that affect the direction of wave packet motion is one of the major purposes of this paper. The diabatic potentials in Figure 2 at first glance imply that the asymmetric stretching motion is dominant because the vertical transition places the wave packet on the circular well potential surface at a position where the motion will be along the line connecting the minima. Indeed, the cross section of the two-dimensional surfaces in our schematic formed the basis of our initial application of time-dependent theory to the intervalence absorption spectrum problem, and also was the basis for most other calculations in the literature.[2,18−22,25,49−51] However, both electronic coupling and vibrational mode coupling prevent the problem from being separated into one-dimensional cross sections. Furthermore, as we show later, symmetric motion of the wave packet can dominate. In the following sections, we delve into the intricacies of the intramolecular forces and interactions that modify the simple schematic in Figure 2.

B. Effect of Different Force Constants. We now examine in more detail the potential energy surface of a single trapped

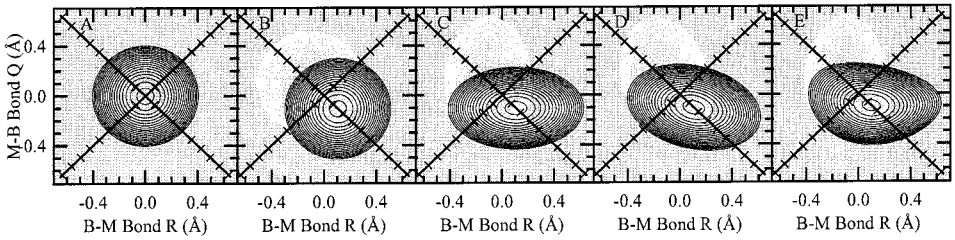

Figure 3. Illustrations of the effects of the coupling terms on the potential energy surfaces. (A) The basic two-dimensional undisplaced harmonic oscillator wells with equivalent force constants. (B) Displacement by Δ_{pot} of the basic circular wells in the asymmetric direction. (C) The effect of coupling k_c between the local coordinates on the shape of the potential. The surfaces become elliptical. (D) The effect of rotation by ϕ on the potential. (E) The effect of anharmonic mode coupling terms on the shape of the potential.

valence form of the molecule and then use the symmetry properties of the molecule to derive the surface for the other state. The molecule with equal M−B bond lengths (the nonmixed valence form of the molecule shown in Figure 1) is the reference configuration for the examination of mixed valence states and defines the zero of the configurational coordinate. Localizing an electron on one site will cause a distortion along that coordinate because of bond-order changes and/or electrostatic effects. The bond length change is represented by the parameter Δ_{pot}. The surface shown in Figures 2 and 3b represents a longer bond along R when the metal is reduced ($\Delta_{pot} > 0$).

Once the molecule is mixed valence, the force constants of the two sites will usually be different. If the "extra" electron is in a bonding orbital it will cause an increase in the force constant k for the reduced site by the amount k_c and a decrease in bond length. Adding an electron into an antibonding orbital results in a reduction in the force constant k by the amount k_c and an increase in bond length. The effect of the change in force constant is to change the potential energy surface from circular to elliptical as illustrated in Figure 3c. The slope of the potential surface is decreased (weaker force constant) along the R local coordinate and increased (strong force constant) along the Q coordinate.

In general the localization of this extra electron can also cause bond length and force constant changes on the other site that will change the force constant and equilibrium nuclear position of the other coordinate. However, because of interchange symmetry, these changes merely represent a change in the reference force constant and equilibrium position from the nonmixed valence species and therefore will not affect the calculation of mixed valence spectra.

C. Local Mode Coupling. The local coordinates on sites Q and R can interact via coupling k_{QR}. If k_{QR} is a constant independent of coordinate then the interaction enters into the potential energy as a term proportional to QR which causes a rotation of the potential energy surface by $2\phi = \arctan(k_{QR}/(k_Q - k_R)) = \arctan(k_{QR}/(2k_c)$. The effect of the coupling on the rotation of the potential energy surface is demonstrated in Figure 3d for $k_{QR} > 0$.

The rotation of the surface changes the relative contribution of the local coordinate from each site to the diabatic normal coordinates. The angle ϕ measures the degree to which the local coordinates couple. The two diabatics, then, have opposite definitions of the amount of each local coordinate that contributes to a given normal coordinate. A wave packet that would be an eigenfunction on one uncoupled diabatic once transferred via coupling to the other surface will find itself on a potential that has undergone a rotation of $\pi/2 - 2\phi$. The angle between the major axes of the ellipses (coordinate of the lower frequency mode or the reduced site for an electron in an antibonding orbital) is $\pi/2$ for no coupling. This limit is appropriate for the case where the mode mixing between coordinates on each site is small. As the angle ϕ is changed from $-\pi/4$ to $\pi/4$, the "symmetric" and "asymmetric" modes swap order energetically for the isolated diabatic potential. When $\phi = -\pi/4$, $\nu_{asym} > \nu_{sym}$, and when $\phi = \pi/4$, $\nu_{sym} > \nu_{asym}$. When $\phi = 0$ $\nu_{sym} = \nu_{asym}$. The limit of $\phi = \pm\pi/4$ is appropriate for strongly coupled local modes. In this case ($\phi = \pm\pi/4$) there is effectively no rotation when the wave packet hops surfaces due to diabatic electronic coupling.

TABLE 1: Symmetry Relationships that Determine the Signs of Molecular Parameters for the Two States by Functional Form of the Potential Energy

function	coeff. sign
$Q^2 + R^2$	same
$Q^2 - R^2$	opposite
$Q + R$	same
$Q - R$	opposite
QR	same

If there are anharmonic effects, that is if the force parameters f_Q and f_R depend on the coordinate, then terms which depend on Q^3 and R^3 must be included. If the force constant representing the interaction between local modes, f_{QR}, depends on coordinate then terms proportional to Q^2R and QR^2 must be included. These parameters cause the surface to lose its ellipticity as illustrated in Figure 3e. We will suppress the cubic and higher order terms for the remainder of this study though their inclusion does not increase computational effort.

There is a symmetry relationship between the two potentials due to the equivalence of the two interchangeable sites. As a result the sign of the coefficients depends on the function of the coordinates they precede. The symmetry relationships between the parameters of the two sites are summarized in Table 1.

D. Diabatic Coupling. The diabatic coupling V_{AB} is the most important part of the Hamiltonian in governing the rate at which the electron is transferred from one site to the other. The electronic coupling results in a break-down of the Born−Oppenheimer separablility of the electronic and nuclear wave functions. The concept of potential surfaces (diabatic and adiabatic) is no longer applicable. Diabatic coupling allows the electron to hop from one state to the other and is a measure of the strength of interaction between the two sites. Large couplings correspond to large interactions that result in strong mixing of the orbitals on each site. The result is delocalized behavior. Weak couplings correspond to localized behavior. Two parameters, ϵ and $\Delta_{coup,}$ together determine V_{AB} and its influence on the spectra. The parameter ϵ measures the strength of the coupling at the origin of the coordinate system and serves as a measure of the overall coupling strength in the system. The electronic coupling will also, in general, be coordinate depend-

TABLE 2: Summary of Parameters Used in Model Hamiltonian of Intervalence Electron Transfer in Two Coordinates

parameter	typical values	description	effect
ϵ	1400 cm^{-1}	constant coupling between states	large values delocalize the electron
k	1.02×10^5 $cm^{-1}/Å^2$ (frequency = 450 cm^{-1})	force constant giving rise to the stated vibrational frequency (mass = 17)	changes spacing of vibrational progression
k_c	0, 25, 50, 100 cm^{-1}	coupling between local coordinates	increases contribution of symmetric coordinate
ϕ	0, 15, 30, 45°	rotation angle of diabatic surfaces	reduces effect of k_c
Δ_{pot}	0, 0.03, 0.06, 0.12, 0.18 Å	bond length distortions in asymmetric coordinate	increases contribution of asymmetric coordinate
Δ_{coup}	0, 0.03, 0.06, 0.12, 0.18 Å	dependence of coupling onthe symmetric coordinate	increases contribution of symmetric coordinate

ent. As the molecule vibrates and the sites come closer together the coupling will increase and vice versa. We account for this behavior by using a coupling that is linear in the symmetric coordinate. The parameter Δ_{coup} measures the degree to which the diabatic coupling depends on symmetric nuclear displacement.

E. The Model Hamiltonian. The final coupled potential energy operator is

$$\hat{\mathbf{V}} = \begin{vmatrix} V_A & V_{AB} \\ V_{BA} & V_B \end{vmatrix}$$

$$V_A = \frac{1}{2}k(Q^2 + R^2) + \frac{1}{2}k_c \cos(2\phi)(Q^2 - R^2) + k_c \sin(2\phi)(QR) + \frac{1}{2}\Delta_{pot}k_c \cos(2\phi)(Q + R) + \frac{1}{2}\Delta_{pot}(k - k_c \sin(2\phi))(Q - R)$$

$$V_B = \frac{1}{2}k(Q^2 + R^2) - \frac{1}{2}k_c \cos(2\phi)(Q^2 - R^2) + k_c \sin(2\phi)(QR) + \frac{1}{2}\Delta_{pot}k_c \cos(2\phi)(Q + R) - \frac{1}{2}\Delta_{pot}(k - k_c \sin(2\phi))(Q - R)$$

$$V_{AB} = V_{BA} = \epsilon - \frac{1}{2}(\Delta_{coup}(k - k_c \sin(2\phi)))(Q + R) \quad (1)$$

In the 2 × 2 matrixes, each diagonal element operates on the nuclear part of the wave function from a single diabatic electronic state whereas the off-diagonal elements transfer population from one state to the other.

3. Analysis of the Contributions of the Symmetric and Asymmetric Modes to Electronic and Resonance Raman Spectra

A. Overview and Scope of the Calculations. The model is designed to incorporate a small number of physically intuitive and calculationally tractable parameters. The five parameters that affect the observed spectra are k, Δ_{pot}, ϵ, Δ_{coup}, k_c, and ϕ. A listing of the parameters, their physical meanings, and their effects on the intensities of the symmetric and asymmetric modes in the spectra is given in Table 2. In this paper, k = 1.02 10^5 $cm^{-1}/Å^2$ and the mass = 17, such that the vibrational frequency in the diabatic potential surface is 450 cm^{-1}. The values of k_c are chosen such that the resulting frequencies change by the stated number of wavenumbers, i.e., k_c = 25 cm^{-1} means that the resulting vibrational frequencies are 425 and 475 cm^{-1}.

The physical insight into the relative importance of the symmetric and asymmetric modes is obtained by interpreting the *direction* of the motion of the wave packet on the surfaces in Figure 2. For example, in Figure 2 (bottom) the initial wave function is found in the minima of the circular potential surfaces. When it is promoted to a high energy part of the other circular potential, the motion will be along the line connecting the minima of the potentials. This line defines the asymmetric vibrational mode. No motion develops in the perpendicular direction (the symmetric mode) and the absorption and resonance Raman spectra will only contain intensity from the asymmetric mode. The couplings that exist in the molecule (both vibrational and electronic coupling) can cause motion to develop in the direction of the symmetric stretch. These effects are developed in detail in the following sections. The following discussion is based on exact calculations for the non Born−Oppenheimer system: we will show how the spectra can smoothly go from symmetric to asymmetric domination as the couplings change.

The usual expectation in resonance Raman and absorption spectra is that the symmetric modes will dominate. However for the simplified picture of intervalence transitions shown in Figure 1 the symmetric mode is not considered. Our model starts with two (uncoupled) local modes (neither symmetric nor antisymmetric). The parameters that control the interaction of the local coordinates to produce the normal coordinates are defined in Table 2 and illustrated in Figure 3. To develop physical insight into how the various couplings affect the motion along the coordinates and hence the symmetric and asymmetric contributions to the spectra, the discussion will emphasize the direction of the wave packet motion.

B. Methodology. *Intervalence Absorption Spectra.* The equation to calculate the frequency domain spectra from time dependent quantum mechanics is[52−55]

$$I(\omega) \propto \omega \int_{-\infty}^{\infty} e^{i\omega t} \langle \Phi \mu | \mu \Phi(t) \rangle dt \quad (2)$$

There are three important quantities in this equation. The first is the initial wave function Φ, the lowest energy eigenfunction of the coupled system. For intervalence transitions involving two coupled diabatic potentials, each eigenfunction at $t = 0$ is an array with two components corresponding to the two diabatic potentials that form the basis in all of the calculations.[20,49,56,57] The second important quantity is the electronic transition dipole moment operator μ: this function operates on both components of the coupled system and promotes the wave packet to the "excited state." The specific functional form of the electronic transition dipole moment operator depends on the symmetry of the molecule involved and the polarization of the light with respect to the molecule. Details of the treatment of the polarization of light and the symmetry considerations have been published.[20,49,58] For the axis system defined in Figure 1, the Z polarization requires an even dipole function whereas the X polarization requires an odd dipole function. The final important quantity is the time evolving correlation function which is calculated using a split operator fast Fourier transform algorithm.[59−62] For two coupled diabatic potential surfaces, the wave packet is a vector quantity with a component for each of the electronic states and is a function of the configurational coordinate Q. As a result, two wave packets moving on the two coupled diabatic potential surfaces are needed.

Intervalence resonance Raman Resonance Raman excitation profiles are calculated in a manner similar to that for absorption spectra. The Raman polarization tensor as a function of

excitation wavelength is given by[63−67]

$$I(\omega_{ex}) \propto \omega_{ex}(\omega_{ex} - \omega_j)^3 \int_0^\infty e^{i\omega_{ex}t}\langle\Phi_{\omega_j}|\Phi(t)\rangle dt \qquad (3)$$

Again, both the propagating wave packet and the dipole moment are important factors. In this case, the dipole "up" is the orientation of the incident light whereas the dipole "down" is the orientation of the scattered light. These dipole functions are the same for the spherical Raman tensor elements *xx*, *zz*, but are different for the Raman tensor elements which give depolarized scattering (*xz*, *zx*). The resonance Raman excitation profile is the intensity of the Raman scattering of a single vibrational mode as a function of excitation wavelength. Typically the resonance Raman excitation profiles will follow the profile of the absorption spectrum with the intensity of the profile being proportional (to first approximation) to the slope of the excited potential in the Condon region. However, the asymmetric bands violate our usual intuition regarding resonance Raman spectra.

C. Analysis of the Effects of Bond Length Changes and Electronic Coupling on the Intensities of the Modes in Absorption and Resonance Raman Spectra. The parameters that have the largest effect on the presence or absence of the symmetric and asymmetric modes are Δ_{pot}, Δ_{coup}, and ϵ. An increase in Δ_{pot} results in an increase in the presence of the asymmetric mode in the spectrum. This increase is expected because an increase in Δ_{pot} causes the surfaces to become displaced further in the asymmetric direction which results in increased motion along the asymmetric coordinate.

The effect of Δ_{pot}, however, is modulated by the electronic coupling; an increase in the coupling will decrease the effective Δ_{pot}. This change occurs because the increase in the coupling increases the delocalization of the system and the nuclei have an increasing share of their probability centered at the origin of the coordinate. Thus, even though the local orbitals involved in the transition may have large changes in the bonding for the modes of interest, strong electronic coupling will "wash out" the nuclear position over the values for both electronic states, effectively reducing the distortion along the asymmetric coordinate and preventing motion of the wave packet from developing in the asymmetric coordinate. The result is that the width of the absorption spectrum will decrease as ϵ increases due to this reduction in the effective Δ_{pot}.

The symmetric mode intensity increases with increasing Δ_{coup}. This parameter is a measure of the change in coupling as the molecule vibrates along the symmetric coordinate. As the sites are brought close together, the coupling increases. As the sites move apart, the coupling decreases. As Δ_{coup} is increased relative to Δ_{pot}, the symmetric mode becomes increasingly important as shown in Figure 4. The top (Figure 4A) and bottom (Figure 4G) parts show the corresponding 1d calculations for the symmetric and asymmetric modes, respectively. These 1d calculations were performed on cuts through the origin along the symmetric and asymmetric coordinates. The absorption spectrum shows an increase in the presence of the symmetric mode with an increase in Δ_{coup}. Note that the spectrum is very sensitive to small increases in Δ_{coup} (e.g., from part F to E of Figure 4 and from part E to D of Figure 4) because wave packet motion increases significantly in the symmetric direction as is discussed more fully in the final paragraph of this section.) In the limit of large Δ_{pot}:Δ_{coup} the spectrum is well modeled by a 1d asymmetric mode calculation. In the limit of small Δ_{pot}:Δ_{coup} the spectrum is well modeled by a 1d symmetric calculation.

The resonance Raman spectra follow this behavior; they show increased scattering intensity for the symmetric mode with an increase in Δ_{coup}. The resonance Raman excitation profiles for three illustrative cases are shown in Figure 5. (Note that these are the scattering cross sections that would be obtained after the absorption kernel from the other displaced modes has been deconvoluted from the excitation profile.) The resonance Raman spectra calculated for excitation near the absorption band maximum are shown in Figure 6 for the same ratios of Δ_{pot}:Δ_{coup} as those in Figure 5.

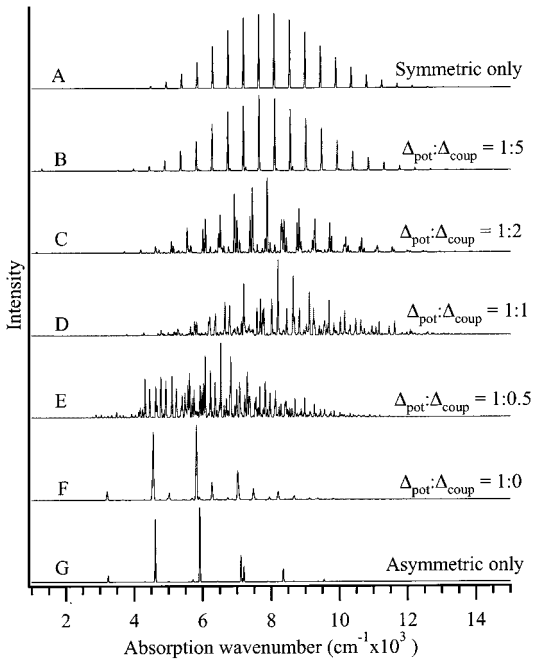

Figure 4. Absorption spectra generated for various ratios of Δ_{pot} and Δ_{coup} as labeled in the figure. In each case the larger of Δ_{pot} and Δ_{coup} is 0.15 Å. Trace A is a one-dimensional harmonic oscillator calculation for a displacement in the symmetric direction equivalent to that implied by the value of $\Delta_{coup} = 0.15$ Å. Trace G is the one-dimensional coupled calculation of the absorption spectrum using the asymmetric mode and neglecting the contribution of the symmetric mode. The values of the other parameters are $k = 1.02 \times 10^5$ cm^{-1}/Å^2 (frequency = 450 cm^{-1}), $m = 17$ amu, $\epsilon = 1400$ cm^{-1}, and $\phi = 0°$. The value of $k_c = 50$ cm^{-1} for B− F and zero for A and G. For A−C the value of $\Delta_{coup} = 0.15$ Å with Δ_{pot} given by the ratio, and for D−F the value of $\Delta_{pot} = 0.15$ Å with Δ_{coup} given by the ratio.

The resonance Raman excitation profiles provide an experimental method of determining the relative importance of the coupling term. The wavelength dependences of the profiles shown in Figure 5 illustrate this point. When the contribution of the Δ_{coup} term is negligible (Figure 5, bottom), the profiles for the symmetric and antisymmetric modes are "nested" and the ratio of the intensities is uniform across the band. The asymmetric mode is the most intense (contrary to the usual expectation of resonantly enhanced modes). In contrast, when Δ_{coup} is significant, the ratio becomes a strong function of the excitation wavelength. An intermediate case is shown in Figure 5 (middle). The maxima of the symmetric and asymmetric profiles do not coincide and the ratio of the intensities changes across the profiles. When the coupling is even larger (in the direction of increasing valence delocalization), the symmetric mode becomes the most intense and the maxima in the excitation profiles are strongly shifted relative to each other.

A more intuitive physical basis for understanding why the coordinate dependence of the coupling causes an increase in the presence of the symmetric mode is available by unitary transformation of the diabatic basis. We showed previously that a unitary transformation takes us from the localized diabatic picture that we have discussed here to a delocalized picture

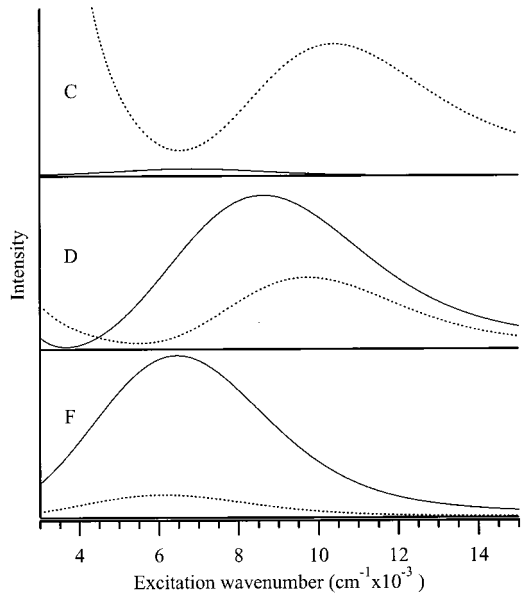

Figure 5. Resonance Raman cross sections calculated for ratios of Δ_{pot} and Δ_{coup} of 1:2 (top), 1:1 (middle), and 1:0 (bottom). The corresponding absorption spectra are shown in Figure 4C, 4D and 4F, respectively. The solid line is the profile for the asymmetric mode and the dashed line is that for the symmetric mode. Note that the positions of the maxima of the profiles are shifted relative to each other when Δ_{coup} is large. The values of the other parameters are the same as those in Figure 4C−F.

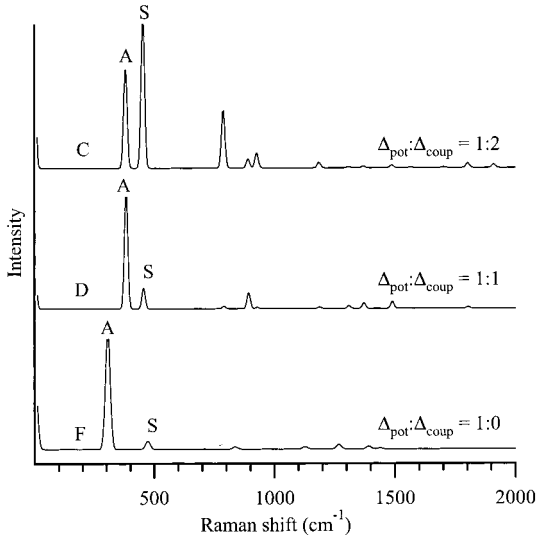

Figure 6. Resonance Raman spectra calculated for the ratios of Δ_{pot} and Δ_{coup} that were used in Figure 5. The excitation wavenumber is that corresponding to the absorption band maxima in Figure 4C,D, and 4F, respectively. The values of the other parameters are $k = 1.02 \times 10^5$ cm^{-1}/Å^2 (frequency = 450 cm^{-1}), $m = 17$ amu, $\epsilon = 1400$ cm^{-1}, and $\phi = 0°$.

where the Δ_{pot} parameter no longer measures a distortion, but measures the strength of the diabatic electronic coupling.[49] By analogy, the reverse transformation from the delocalized picture to the localized picture results in the distortion along the symmetric coordinate becoming the slope of the coupling with respect to the symmetric coordinate in the localized picture. Similarly, unitary transformation to the adiabatic representation results in displacements of the surfaces along the symmetric coordinate by $\pm\Delta_{coup}$. Therefore, Δ_{coup} measures an effective coordinate displacement in the symmetric coordinate and serves also to measure the coordinate dependence of the coupling

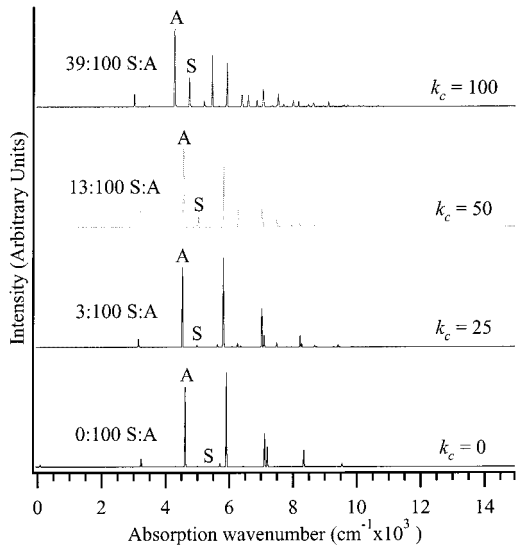

Figure 7. Effect of the coupling on the absorption spectrum. Absorption spectra are calculated using $k_c = 0$, 25, 50, and 100 cm^{-1} as labeled in the figure. The ratio of the asymmetric (A) (2,0) to the symmetric (S) (2,1) band is given at the left of each spectrum and illustrates the increasing contribution of the symmetric mode with increasing k_c. The values of the other parameters are $k = 1.02 \times 10^5$ cm^{-1}/Å^2 (frequency = 450 cm^{-1}), $m = 17$ amu, $\epsilon = 1400$ cm^{-1}, and $\phi = 0°$.

between the two sites as the molecule is stretched along the symmetric combination of local coordinates.

D. Effects of the Nonequivalence of Local Coordinate Force Constants. The next parameter that is examined is k_c, the difference between the force constants of the local coordinate on the oxidized site and the local coordinate on reduced site. For large values of this parameter the wave packet experiences a large change in local force constant as the electron moves from one site to the other (that is, as the wave packet moves from one surface to the other). As a simple example, when the wave packet is placed on the opposite potential surface in Figure 3c, the motion is no longer purely in a straight line toward the minimum along the asymmetric coordinate, but also develops motion along the symmetric coordinate. Thus, the intensity of features from the symmetric coordinate will increase as the surfaces become more elliptical with increasing k_c,.

The absorption spectra generated by varying k_c such that the changes in the vibrational frequencies are 25, 50 and 100 cm^{-1} are shown in Figure 7. This figure demonstrates the increase in the contribution of the symmetric coordinate. The $v = (0,2)$ and $v = (1,2)$ bands are marked with an "A" and an "S" respectively in the spectra. As the contribution of the symmetric mode increases the intensity of S will increase with respect to A.

Resonance Raman excitation profiles provide a more sensitive measure of the relative contribution of each mode. An unstructured absorption spectrum is rather insensitive to the k_c parameter; the overall width of the spectrum is only slightly affected. The resonance Raman spectra generated by varying k_c such that the changes in the vibrational frequencies are 25, 50, and 100 cm^{-1} are shown in Figure 8. When $k_c = 0$ the asymmetric band is the most intense and the symmetric band is not observed. As k_c increases, the symmetric band grows in (ca. 500 cm^{-1} in Figure 8).

The coupling parameter ϵ modulates the effect of k_c because it reduces the localization of the system. When the system is delocalized, the lowest energy eigenfunction has most of its probability amplitude near the crossing region and therefore has

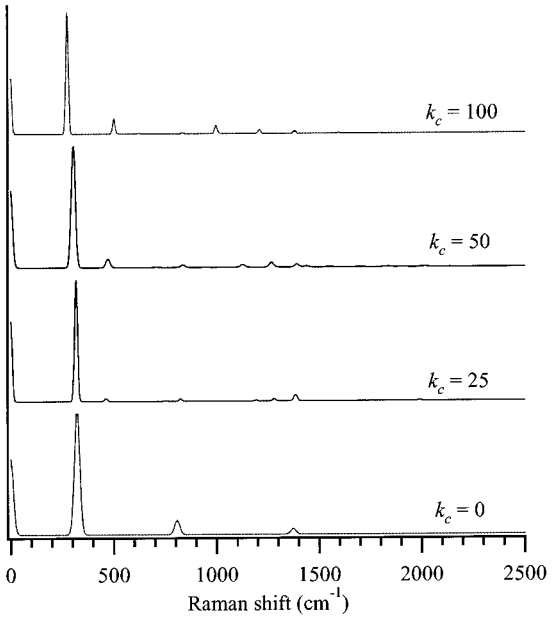

Figure 8. Effect of the coupling on the resonance Raman spectrum. The spectra are calculated using $k_c = 0$, 25, 50, and 100 cm^{-1}. The asymmetric band is the intense band at ca. 300 cm^{-1}; the symmetric band grows in (ca. 500 cm^{-1}) as k_c increases. The values of the other parameters are $\Delta_{coup} = 0.15$ Å, $\Delta_{pot} = 0$ Å, $k = 1.02 \times 10^5$ cm^{-1}/Å^2 (frequency = 450 cm^{-1}), $m = 17$ amu, $\epsilon = 1400$ cm^{-1}, and $\phi = 0°$.

a more averaged local force constant. For the value of ϵ that we use for this comparison (1400 cm^{-1}), the system is intermediate between localized and delocalized. Therefore there is significant probability amplitude both in and away from the crossing region.

E. Effect of the Nonequivalence of Normal Coordinate Force Constants. The last parameter we will examine is ϕ, the rotation of the diabatic surfaces. As the surfaces rotate, the relative contributions of the symmetry coordinates to the normal coordinates for a given diabatic change. If there is no difference in force constant the rotation of the diabatic has no effect. For k_c causing a change in the vibrational frequency of 50 cm^{-1}, we examine the effect of changing ϕ from 0 to $\pi/4$ ($\phi = 0°$, 15°, 30°, and 45°.) Because this parameter reduces the local effective force constant change that the nuclei experience when the electron changes sites, the amount of symmetric coordinate contribution (absorption) and enhancement (resonance Raman) will decrease as ϕ increases from 0 to $\pi/4$. This decrease is observed in the absorption spectra in Figure 9. In Figure 10 the resonance Raman scattering excitation profiles exhibit a similar trend.

Effects of the Interaction of k_c and ϕ. The parameter k_c is a measure of the difference between the force constants. In effect it is the measure of the amount of change in bonding interaction that occurs on one site when the electron is removed from the orbital in question. Thus it is also a measure of the degree to which the electron transfer is coupled to the motion of the nuclei. As was discussed earlier, an increase in this parameter increases the local mode behavior of each electronic state and results in an increased intensity of the symmetric mode in the spectra. The increase effectively causes a force constant change in the local coordinate directions after the transition to the other surface. That force constant change allows wave packet motion to occur along the symmetric direction because motion in that direction must occur if the wave packet is to "relax" to is the favored geometry in the new electronic state.

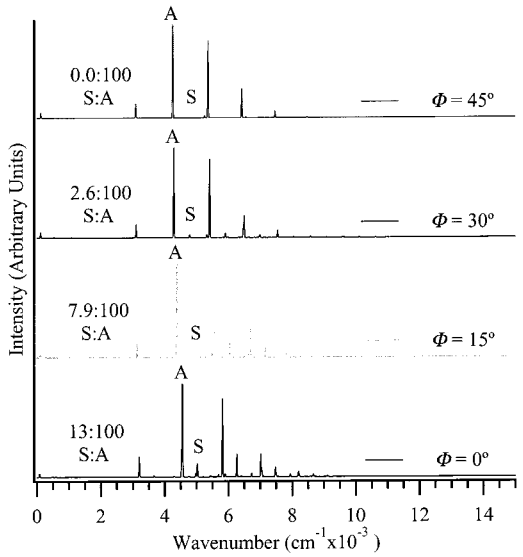

Figure 9. Effect of the rotation angle of the diabatic surfaces on the absorption spectrum. Absorption spectra are calculated using values of $\phi = 0°$, 15°, 30°, and 45° as labeled in the figure. The values of the other parameters are $\Delta_{coup} = 0.15$ Å, $\Delta_{pot} = 0$ Å, $k = 1.02 \times 10^5$ cm^{-1}/Å^2 (frequency = 450 cm^{-1}), $m = 17$ amu, $\epsilon = 1400$ cm^{-1}, $\phi = 0°$, and $k_c = 50$ cm^{-1}.

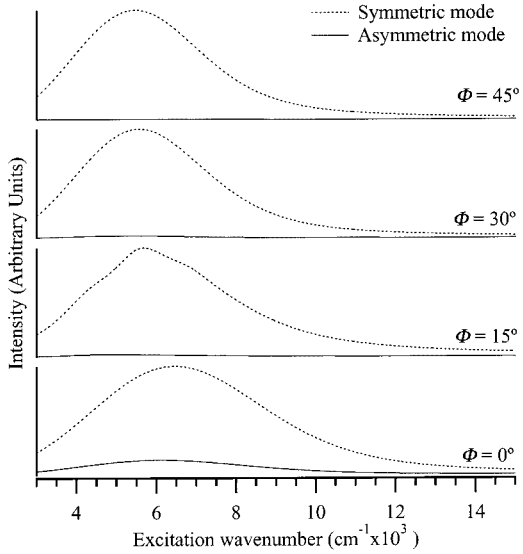

Figure 10. Effect of the rotation angle of the diabatic surfaces on the resonance Raman cross sections. Cross sections for the symmetric (dotted lines) and asymmetric (solid lines) normal modes are calculated using values of $\phi = 0$, 15, 30, and 45° as labeled in the figure. The values of the other parameters are $\Delta_{coup} = 0.15$ Å, $\Delta_{pot} = 0$ Å, $k = 1.02 \times 10^5$ cm^{-1}/Å^2 (frequency = 450 cm^{-1}), $m = 17$ amu, $\epsilon = 1400$ cm^{-1}, and $k_c = 50$ cm^{-1}.

The parameter ϕ modulates the effect of k_c by reducing the local mode behavior and returning normal mode behavior. Since the wave packet is aligned increasingly along normal modes with an increase in the magnitude of ϕ to $\pi/4$ there is less motion along the symmetric coordinate until ultimately at $\phi = \pm\pi/4$ the motion along the symmetric coordinate is completely suppressed. Note that an increase in coupling ϵ also reduces the effect of k_c but cannot completely eliminate it.

F. Limiting Spectra. When only the constant coupling term ϵ is used to calculate the spectra ($\Delta_{coup} = 0$) and all interactions between vibrational modes are ignored ($k_c = 0$ and $\phi = 0$), the spectra take on the form expected from one-dimensional calculations that use only the asymmetric coordinate.[18,20,45]

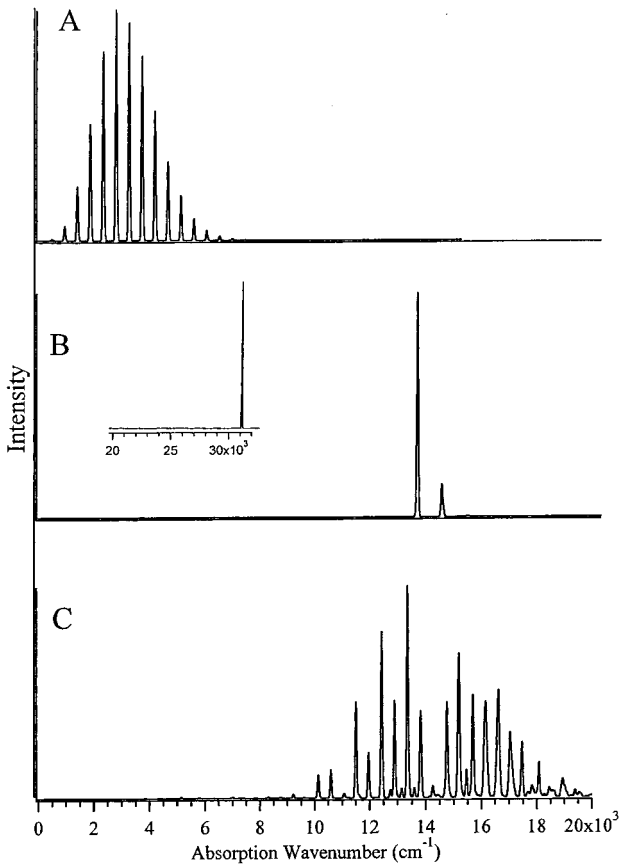

Figure 11. Examples of limiting spectra. (A) Spectra for a localized system ($\epsilon = 10$ cm^{-1}) when only the constant coupling term ϵ is used to calculate the spectra ($\Delta_{coup} = 0$) and all interactions between vibrational modes are ignored ($k_c = 0$ and $\phi = 0$). (B) Spectrum of a delocalized system ($\epsilon = 9000$ cm^{-1}) when only the constant coupling term ϵ is used to calculate the spectra ($\Delta_{coup} = 0$) and all interactions between vibrational modes are ignored ($k_c = 0$ and $\phi = 0$). An extreme ($\epsilon = 15000$ cm^{-1}), is shown in the insert. (C) Spectrum of a delocalized molecule when the coordinate dependent coupling is nonzero (Δ_{pot}: $\Delta_{coup} = 1{:}5$) and $\epsilon = 9000$ cm^{-1}. The values of the other parameters in A−C are $\Delta_{pot} = 0.15$ Å, $k = 1.02\ 10^5$ cm^{-1}/Å^2 (frequency = 450 cm^{-1}), $m = 17$ amu, and $k_c = 0$ cm^{-1}.

Spectra that are calculated for z polarization using two values of the coupling, one small ($\epsilon = 10$ cm^{-1}) and one large ($\epsilon = 9000$ cm^{-1}) are shown in Figures 11A,B, respectively. The spectra are dominated by the asymmetric mode. As the coupling increases, the spectra become increasingly narrow and the transition energies approach twice the coupling plus the difference between the zero-point energies. An extreme case ($\epsilon = 15{,}000$ cm^{-1}) is shown in the inset to Figure 11B. When the constant coupling is large (representing a delocalized molecule) and the coordinate dependent coupling is nonzero, the spectra become dominated by and broadened by the progression in the symmetric mode. An example (Δ_{pot}:$\Delta_{coup} = 1{:}5$ and $\epsilon = 9000$ cm^{-1}) is shown in Figure 11C. These trends can be interpreted in terms of the direction of the motion of the wave packet as discussed above. When $\Delta_{coup} = 0$, the wave packet motion is primarily between the minima of the potential surfaces and along the asymmetric coordinate (Figure 11A). When the coupling is large, very little wave packet motion occurs and the spectrum is sharp. Thus when the constant coupling is large and there is also coordinate dependent coupling, increasing the latter increases wave packet motion in the symmetric direction and the symmetric stretch becomes increasingly important in the spectrum.

4. Summary

Both symmetric and asymmetric normal modes can contribute to intervalence absorption spectra. In addition, both types of modes can have appreciable intensities in resonance Raman spectra taken in resonance with the intervalence transition. Depending on the interactions in the molecule, either type of mode can dominate the spectrum. This result is surprising because the standard approach to treating intervalence transitions places emphasis on the asymmetric coordinate whereas the standard approach to electronic and resonance Raman spectroscopy predicts that highly displaced symmetric modes will dominate the spectra. Generally, the intervalence absorption spectra are broad and do not reveal the relative importance of the two types of modes. In contrast, Raman spectra are very sensitive and provide much more information about the symmetry of the modes and thus the interactions in the molecule.

The relative intensities of the symmetric and asymmetric modes are most sensitive to the interplay between the electronic coupling between the sites (ϵ), the changes in bond lengths that occur when the electron is transferred (Δ_{pot}) and the sensitivity of the coupling to the distance between the electron-transfer centers (Δ_{coup}). In strongly delocalized systems (large ϵ) the symmetric mode will be prominent. For a given ϵ, the more sensitive the bond length to the change in the charge after electron transfer the more intense the asymmetric mode. The more sensitive the coupling to the distance between the sites, the more intense the symmetric mode. The physical meaning of these trends are readily visualized by the direction of the motion of the wave packet on the coupled potential surfaces. The relative intensities are dependent upon, but are less sensitive to, the local vibrational mode coupling. The trends required for an increase in the symmetric mode are an increase in k_c the difference in the force constant, and a decrease in Φ, the rotation of the diabatic surfaces.

Quantitative fitting of spectra must be approached and interpreted carefully because of the large number of important and interacting parameters present even in a simple two-dimensional model. However, the trends that are measured in a series of compounds can reveal the most important interactions in the molecules. The most general result from our calculations is that the more delocalized the system, the more important the contribution of the symmetric modes to the spectra, and vice versa. Detailed understanding of mixed valence molecules will require the combination of multiple spectroscopies to fully determine the vibronic Hamiltonian.

Acknowledgment. This work was supported by a grant from the National Science Foundation (CHE-9816552).

Supporting Information Available: Calculation of intervalence spectra using the time-dependent theory of spectroscopy. This material is available free of charge via the Internet at http://pubs.acs.org.

References and Notes

(1) Robin, M. B.; Day, P. *Adv. Inorg. Chem. Radiochem.* **1967**, *10*, 247.
(2) Brown, D. B. *Mixed Valence Compounds*; Reidel: Dordrecht, 1980.
(3) Allen, G. C.; Hush, N. S. *Prog. Inorg. Chem*. **1967**, *8*, 357.
(4) Hush, N. S. *Chem. Phys.* **1975**, *10*, 361−6.
(5) Hush, N. S. *Coord. Chem. Rev*. **1985**, *64*, 135.
(6) Creutz, C. *Prog. Inorg. Chem.* **1983**, *30*, 1.
(7) Crutchley, R. J. *Adv. Inorg. Chem.* **1994**, *41*, 273.
(8) Blasse, G. *Struct. Bonding* **1991**, *76*, 153.
(9) Taylor, P.; Beattie, J. K.; Hush, N. S. *Inorg. Chem.* **1976**, *15*, 992.
(10) Bersuker, I. B.; Borshch, S. A. *Adv. Chem. Phys.* **1992**, *81*, 703.

(11) Wieghardt, K. *Angew. Chem.* **1989**, *28*, 1153.
(12) Kaim, W.; Klein, A.; Glockle, M., *Acc. Chem. Res*. **2000**, 33, 755.
(13) Vincent, J. B. *Adv. Inorg. Chem.* **1989**, *33*, 197.
(14) Demadis, K. D.; El-Samanody, E.-S.; Coia, G. M.; Meyer, T. J. *J. Am. Chem. Soc*. **1999**, *121*, 535−544.
(15) Demadis, K.; Neyhart, G.; Kober, E.; White, P.; Meyer, T. *Inorg. Chem.* **1999**, *38*, 5948.
(16) Williams, R.; Petrov, V.; Lu, H.; Hupp, J. *J. Phys. Chem. A* **1997**, *101*, 8070.
(17) Karki, L.; Williams, R.; Hupp, J.; Allan, C.; Spreer, L. *Inorg. Chem.* **1998**, *37*, 2837.
(18) Piepho, S. B.; Krausz, E. R.; Schatz, P. N. *J. Am. Chem. Soc*. **1978**, *100*, 2996.
(19) Wong, K. Y.; Schatz, P. N.; Piepho, S. B. *J. Am. Chem. Soc*. **1979**, *101*, 2793.
(20) Simoni, E.; Reber, C.; Talaga, D.; Zink, J. I. *J. Phys. Chem.* **1993**, *97*, 12678.
(21) Talaga, D. S.; Reber, C.; Zink, J. I. *J. Phys. Chem.* **1994**, *98*, 11233.
(22) Schatz, P. N.; Piepho, S. B. *J. Phys. Chem* **1994**, *98*, 11226−11229.
(23) Reimers, J. R.; Hush, N. S., *Chem. Phys*. **1996**, *208*, 177−193.
(24) Hush, N. S., *NATO Adv. Study Ser*. **1982**, *198*, 151.
(25) Peipho, S. B. *J. Am. Chem. Soc*. **1988**, *110*, 6319.
(26) Piepho, S. B. *J. Am. Chem. Soc*. **1990**, *112*, 4197.
(27) Dong, Y. H.; Hupp, J. T.; Yoon, D. I. *J. Am. Chem. Soc*. **1993**, *115*, 4379.
(28) Hong, L.; Petrov, V.; Hupp, J. T. *Chem. Phys. Lett.* **1995**, *235*, 521.
(29) Hupp, J. T.; Dong, Y. H. *Inorg. Chem.* **1994**, *33*, 4421−4424.
(30) Petrov, V.; Hupp, J. T.; Mottley, C.; Mann, L. C. *J. Am. Chem. Soc.* **1994**, *116*, 2171.
(31) Roberts, J. A.; Hupp, J. T. *Inorg. Chem.* **1992**, *31*, 157−160.
(32) Hornung, F.; Baumann, F.; Kaim, W.; Olabe, J.; Slep, L.; Fiedler, J. *Inorg. Chem.* **1998**, *37*, 311.
(33) Ko, J.; Ondrechen, M. J. *Chem. Phys. Lett.* **1984**, *112*, 507−12.
(34) Ferretti, A.; Lami, A.; Ondrechen, M. J.; Villani, G. *J. Phys. Chem.* **1995**, *99*, 10484.
(35) Ondrechen, M. J.; Ferretti, A.; Lami, A.; Villani, G. *J. Phys. Chem.* **1994**, *98*, 11230.
(36) Ondrechen, M. J.; Ko, J.; Root, L. J. *J. Phys. Chem.* **1984**, *88*, 5919−23.
(37) Lu, H.; Petrov, V.; Hupp, J. T. *Chem. Phys. Lett*. **1995**, *235*, 521.
(38) Williams, R. D.; Hupp,. T.; Ramm, M. T.; Nelsen, S. F. *J. Phys. Chem*. **1999**, *103*, 11172.
(39) Burghardt, I.; Meyer, H.-D.; Cederbaum, L. S. *J. Chem. Phys*. **1999**, *111*, 2927.
(40) Worth, G. A.; Meyer, H.-D.; Cederbaum, L. S. *Chem. Phys. Lett*. **1999**, *299*, 451.
(41) Raab, A.; Worth, G. A.; Meyer, H.-D.; Cederbaum, L. S. *J. Chem. Phys*. **1999**, *110*, 936.
(42) Worth, G. A.; Meyer, H.-D.; Cederbaum, L. S. *J. Chem. Phys*. **1998**, *109*, 3518.
(43) Koeppel, H.; Domcke, W.; Cederbaum, L. S. *Adv. Chem. Phys*. **1984**, *57*, 59.
(44) Cromp, B.; Triest, M.; Carrington, T., Jr.; Reber, C. *Spectrochim. Acta, Part A* **1999**, *55A*, 575.
(45) Savoie, C.; Reber, C. *J. Am. Chem. Soc*. **2000**, *122*, 844.
(46) Stock, G.; Woywod, C.; Domcke, W.; Swinney, T.; Hudson, B. S. *J. Chem. Phys*. **1995**, *103*, 6851.
(47) Stock, G.; Domcke, W. *J. Chem. Phys*. **1990**, *93*, 5496.
(48) Pacher, T.; Cederbaum, L. S.; Köppel, H. *Adv. Chem. Phys*. **1993**, *84*, 293.
(49) Talaga, D. S.; Zink, J. I. *J. Phys. Chem.* **1996**, *100*, 8712.
(50) Prassides, K.; Schatz, P. N. *J. Phys. Chem.* **1989**, *93*, 8387.
(51) Triest, M.; Davis, M. J.; Reber, C. *New J. Chem.* **1999**, *23*, 425.
(52) Heller, E. J. *Acc. Chem. Res.* **1981**, *14*, 368.
(53) Heller, E. J. *J. Chem. Phys.* **1975**, *62*, 1544.
(54) Heller, E. J. *J. Chem. Phys.***1978**, *68*, 3891−6.
(55) Zink, J. I.; Shin, K. S. *Adv. Photochem.* **1991**, *16*, 119.
(56) Heather, R.; Metiu, H. *J. Chem. Phys.* **1989**, *90*, 6903.
(57) Alvarellos, J.; Metiu, H. *J. Chem. Phys.* **1988**, *88*, 4957.
(58) Zhang, J. Z.; Heller, E. J.; Huber, D.; Imre, D. G. *J. Phys. Chem*. **1991**, *95*, 6129.
(59) Feit, M. D.; Fleck, J. A., Jr.; Steiger, A. *J. Comput. Phys.* **1982**, *47*, 412−33.
(60) Kosloff, R.; Ratner, M. A. *J. Chem. Phys.* **1982**, *77*, 2841.
(61) Kosloff, D.; Kosloff, R. *J. Comput. Phys.* **1983**, *52*, 35.
(62) Tanner, J. J. *J. Chem. Educ.* **1990**, *67*, 917.
(63) Tannor, D. J.; Sundberg, R. L.; Heller, E. J. *J. Phys. Chem.* **1982**, *86*, 1822.
(64) Shin, K. S. K.; Clark, R. J. H.; Zink, J. I. *J. Am. Chem. Soc.* **1990**, *112*, 3754.
(65) Reber, C.; Zink, J. I. *J. Chem. Phys.* **1992**, *96*, 2681.
(66) Reber, C.; Zink, J. I. *J. Phys. Chem*. **1992**, *96*, 571.
(67) Wexler, D.; Zink, J. I.; Reber, C. *J. Phys. Chem*. **1992**, *96*, 8757.